Lyapunov-Based Nonlinear Observer Design for an Inductively Supplied Saturated Excitation Coil of an Externally Excited Synchronous Machine

Stefan Köhler, Bernhard Wagner
Laboratory for Control Technology
Technische Hochschule Nürnberg GSO
Nuremberg, Germany
stefan.koehler@th-nuernberg.de
bernhard.wagner@th-nuernberg.de

Stefan Endres, Christoph Seßler
Vehicle Electronics: Battery Chargers
Fraunhofer IISB
Erlangen, Germany
stefan.endres@iisb.fraunhofer.de
christoph.sessler@iisb.fraunhofer.de

***Abstract*—An inductive energy transfer system (IETS) for the energy supply of the excitation coil of an externally excited synchronous machine (EESM) has been developed. Due to the removal of the slip rings, it is impossible to measure the excitation current and the rotor resistance on the rotating rotor. Therefore, a nonlinear observer for the EESM with IETS is presented, which estimates the excitation current and the rotor resistance. This observer is designed with the direct method of Lyapunov.**

Keywords—externally excited synchronous machine; electric mobility; drive control; inductive energy transfer; direct method of Lyapunov; nonlinear observer

I. INTRODUCTION

Since the beginning of the energy turnaround the demand for electric vehicles has been grown increasingly and the automotive industry is permanently searching for more efficient technologies in the area of electric mobility. The interest in this topic is higher than ever and therefore, a wide spectrum of research is done to improve electric machines.

Most concepts regarding their drives primarily utilize asynchronous machines (ASM) and permanent magnet synchronous machines (PSM). Nevertheless, the comparison between these two machine types with the electrically excited synchronous machine (EESM) shows that latter represents a better drive solution, at least for axle drives. The EESM achieves a high to very high efficiency for the whole speed and torque range as shown in Figure 1 [1].

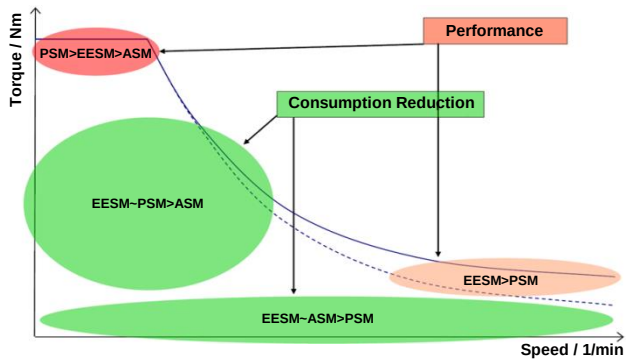

Figure 1: Qualitive comparison of the efficiency (EESM-PSM-ASM)

On the contrary to the permanently excited synchronous machine its excitation system does not require expensive rare earth magnets. Instead, an excitation coil is used, which power is normally supplied by a slip ring unit. This energy transmission component leads to mechanical wear and consequently to an abrasion in the air gap. Thus, high voltage insulation problems may occur.

The project FORELMO, funded by the Bavarian Research Association, was established, which deal with the whole drive train of an EESM. One subproject investigates the energy supply of the excitation coil of the EESM by an inductive energy transfer system (IETS). This study comprised the choice of the DC/DC converter type, the design of the converter as well as the design of its rotary transformer, the control concept and the estimation algorithm of the excitation current and the rotor resistance of the excitation coil.

This paper presents a Lyapunov-based nonlinear observer for the rotor of the EESM as described in [2] with an IETS for the rotor excitation energy as presented in [3]. The estimation algorithm is important, because it would be a huge effort to take measurements on the rotating rotor. The excitation current estimation is necessary for control purposes, whereas the estimation of the rotor resistance is needed to protect the EESM against overheating. The investigations are done with a standard electric vehicle traction EESM with the following key data:

- Max. mechanical engine power: $P_{engine,max}$ = 60 kW
- Max. rotational speed: n_{rotor} = 12500 min^{-1}
- DC input voltage range: U_{Bat} = 250 V…400 V
- Max. excitation power: $P_{exc,max}$ = 2 kW
- Excitation current range: I_{exc} = 3 A…16 A
- Rotor resistance range: R_{exc} = 7,5 Ω…11,5 Ω (over temperature)
- Rotor inductance range: L_{exc} = 0,3 H…0,8 H (under saturation).

II. Structure of the Developed Inductive Energy Transfer System

The simplified structure of the IETS is shown in Figure 2. The abbreviations mean:

- Bat – Battery
- BC – Buck Converter
- CLL RC – CLL Resonant Converter
- EC – Excitation Coil
- Ch – Chopper
- ResCirc – Resonant Circuit
- RotTr – Rotary Transformer
- FB RF – Full Bridge Rectifier
- SC – Smoothing Capacitor
- PrimC – Primary Core
- SecC – Secondary Core.

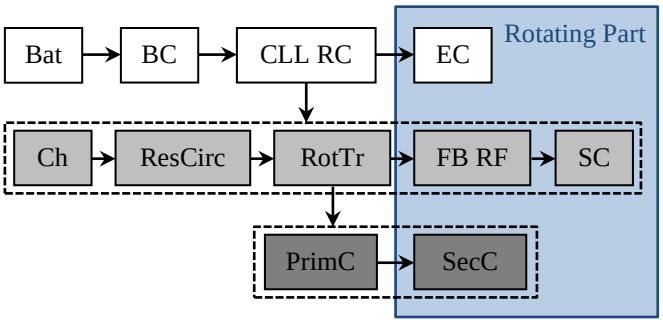

Figure 2: Schematic structure of the inductive energy transfer system

A. Converter Concept

As depicted in Figure 2 the developed IETS is a two stage concept consisting of a BC and a CLL RC. The CLL RC operates with a constant switching frequency f_s, which is equal to the upper resonant frequency f_0. This operating point presents a voltage ratio of 1:1. Here, the CLL RC has the lowest switching losses [4]. The BC controls the IETS by its duty cycle D_{buck}. The electrical equivalent circuits of the BC and the CLL RC are shown in Figure 3 and Figure 4 with the following components:

1 Connection to the battery (U_{Bat})
2 DC link capacitor of the BC ($C_{DC,buck}$)
3 Chopper of the BC → Control of the IETS by the duty cycle D_{buck} of the BC
4 Freewheeling diode
5 Low pass filter ($L_{f,buck}$, $C_{f,buck}$)
6 Connection to the CLL RC (u_{buck})
7 Connection to the BC (u_{buck})
8 DC link capacitor of the BC ($C_{DC,CLL}$)
9 Chopper of the CLL RC
10 Resonant capacitor (C_{res})
11 Rotary transformer (L_σ, L_h)
12 Full bridge rectifier
13 Smoothing capacitor (C_{sm})
14 Excitation coil (R_{exc}, L_{exc}).

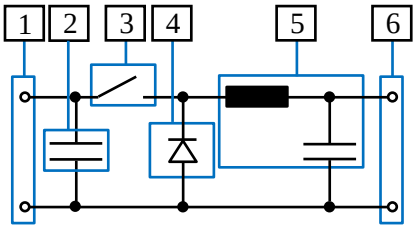

Figure 3: Electrical equivalent circuit of the buck converter

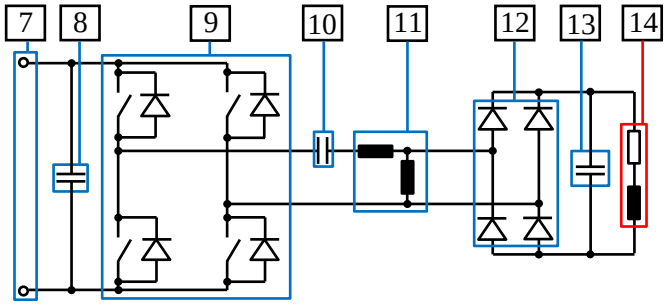

Figure 4: Electrical equivalent circuit of the CLL resonant converter

This two stage variant was chosen, because it is almost impossible to cover the whole output voltage range of 7,5 V…120 V (R_{exc} = 7,5 Ω) with a single CLL RC, which is controlled by the switching frequency. The reason for that is the small negative slope for high switching frequencies. Beside the preferred variant diverse other concepts were investigated, which are summarized in Table I in conjunction with their exclusion criteria.

Table I: Additional concepts for the realization of the IETS and their exclusion criteria

Concept	Exclusion Criteria
Phase Shift Converter	- Huge voltage overshoot on the secondary side - Snubber required → Additional components on the rotor (resistor and capacitor, preferred variant: only an additional capacitor is needed) → Efficiency decreases
Huge additional resonant inductance as described in [5]	- Significantly larger build space required
Operation concepts: CLL RC with phase shift operation, CLL RC with burst mode	- Compared to the two stage variant: Lower efficiency over the whole operational range (cf. Figure 5)

Figure 5 shows the comparison of the efficiency between the CLL RC with burst mode, the CLL RC with phase shift operation and the CLL RC with BC. The CLL RC with BC achieves the best efficiency over the whole operational range. The maximum reached efficiency regarding to the preferred converter concept amounts 93 %, whereas the maximum efficiency of the other both concepts remains below 92 %.

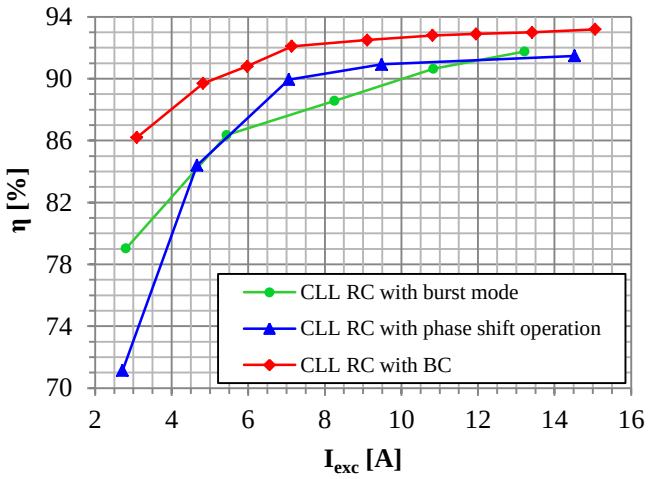

Figure 5: Comparison of the efficiency

B. Rotary Transformer

Figure 6 shows a principle drawing, the manufactured ferrite cores and a FEM analysis of the rotary transformer. The detailed description regarding the core geometry, the design and measurement results were published in [3].

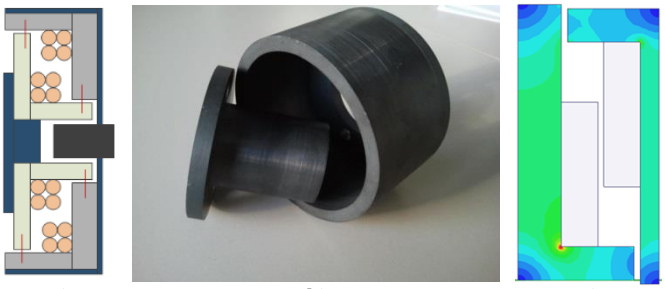

Figure 6: a) Principle drawing b) Manufactured ferrite cores c) FEM analysis of the rotary transformer

III. Lyapunov-Based Nonlinear Observer

The direct method of Lyapunov is used for the design of the nonlinear observer to ensure a stable estimation. Figure 7 shows its simplified structure. The input parameters are the measured output current i_{buck} and the measured output voltage u_{buck} of the BC. By using the calculated excitation voltage $u_{exc,x}$ for the parallel model of the excitation coil the estimated excitation current $\hat{i}_{exc}$ is determined. The calculated excitation current $i_{exc,x}$ serves as reference for the comparison with the excitation current from the parallel model $\hat{i}_{exc}$. The dynamics of the estimation of the rotor resistance depends on the correction factor h_R. The outputs of the nonlinear observer are the estimated excitation current $\hat{i}_{exc}$ and the estimated rotor resistance $\hat{R}_{exc}$.

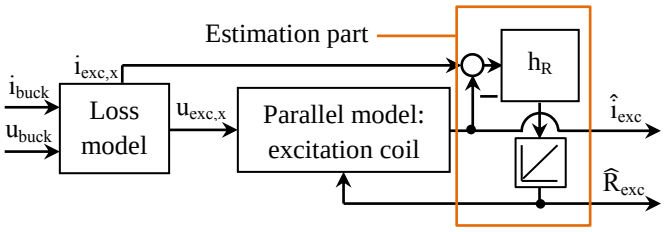

Figure 7: Simplified structure of the Lyapunov-based nonlinear observer for the estimation of the excitation current and the rotor resistance of the EESM

A. Nonlinear Model of the Excitation Coil

The excitation coil, which is represented by an ohmic-inductive load, possesses a nonlinear system behavior because of the excitation current dependent rotor inductance L_{exc}. Figure 8 shows measurement results, which quantify the rotor inductance for different values of the excitation current. It can be seen, that the rotor inductance significantly decreases with the increase of the excitation current. At an excitation current of 16 A there is a rotor inductance of 0,3 H, which is only 37,5 % of the maximum value. Hence, this effect is not negligible.

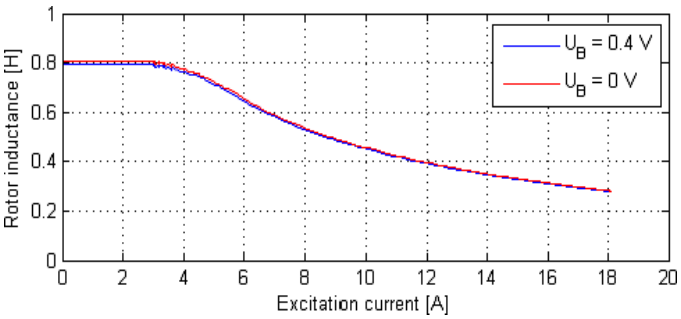

Figure 8: Measurement of the rotor inductance for different values of the excitation current

This effect must be taken into consideration in the mathematical model and the control algorithm. It follows

$$u_{exc}(t)=R_{exc}(t)\cdot i_{exc}(t)+\dot{\psi}_{exc}(t). \quad (1)$$

Assuming that $I_d = 0$ A, the magnetic flux ψ_{exc} result in

$$\psi_{exc}(t)=L_{exc}(i_{exc}(t))\cdot i_{exc}(t). \quad (2)$$

From equation (2) it follows the nonlinear differential equation of the magnetic flux

$$\dot{\psi}_{exc}(t)=\left(L_{exc}(i_{exc}(t))+\frac{dL_{exc}(i_{exc}(t))}{di_{exc}(t)}\cdot i_{exc}(t)\right)\cdot\frac{di_{exc}(t)}{dt}. \quad (3)$$

For the sake of clarity the time dependency (t) is omitted in the further explanations of this paper. Figure 9 shows the comparison of the measured excitation current with the simulated

excitation current. It can be seen, that the simulation result well reproduces the real progression of the excitation current. In consideration of the excitation current dependent rotor inductance, the derived model of the excitation coil creates a good basis for the further investigations.

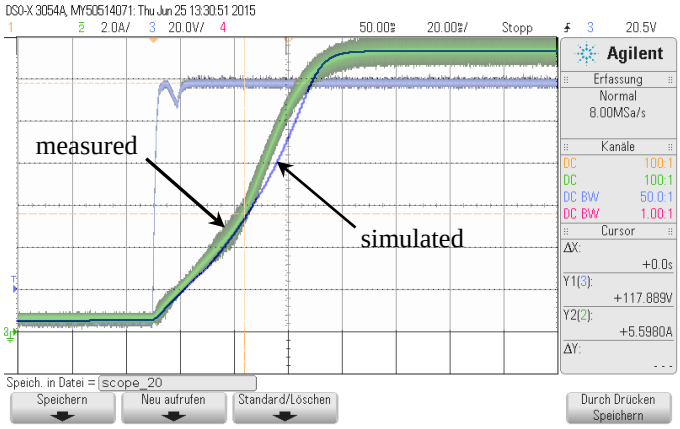

Figure 9: Comparison of the progression of the measured excitation current with the progression of the simulated excitation current (step of the excitation voltage from 5 V…120 V → 0,56 A…13,2 A)

B. *State Equations*

Now, the state equations can be derived. These differential equations treat the rotor resistance R_{exc} as additional state variable beside the excitation current. Hence, an approach is created, which allowed the estimation of the rotor resistance. With equation (1) and (3) the differential equations for the real and the modelled excitation current result in

$$\frac{di_{exc}}{dt}=\frac{1}{L_{exc}(i_{exc})+\frac{dL_{exc}(i_{exc})}{di_{exc}}\cdot i_{exc}}\cdot(u_{exc}-R_{exc}\cdot i_{exc}) \tag{4}$$

and

$$\frac{d\hat{i}_{exc}}{dt}=\frac{1}{L_{exc}(\hat{i}_{exc})+\frac{dL_{exc}(\hat{i}_{exc})}{d\hat{i}_{exc}}\cdot \hat{i}_{exc}}\cdot(u_{exc}-\hat{R}_{exc}\cdot\hat{i}_{exc}). \tag{5}$$

It becomes apparent, that there are different nonlinearities regarding to equation (4) and (5). Therefore, a nonlinear observer is required. In the following, it is assumed that the denominators of equation (4) and (5) are equal, because of the chosen control method: Here, the exact linearization and the trajectory planning are applied [6]. Therefore, the real excitation current and the estimated excitation current will follow the reference trajectory in a similar way. Consequently, the estimated excitation current is always near the real excitation current. To simplify the notation of the following equations the denominator is now written as f_L. The differential equations for the real and the modelled rotor resistance result in

$$\frac{dR_{exc}}{dt}=0 \tag{6}$$

and

$$\frac{d\hat{R}_{exc}}{dt}=h_R\cdot(i_{exc}-\hat{i}_{exc}). \tag{7}$$

C. *Calculation of the Correction Factor h_R with the Direct Method of Lyapunov*

For the identification of a suitable correction factor h_R the direct method of Lyapunov is used, which represents a stability analysis for nonlinear systems. The general theory for the following investigations is explained in detail in [7]. An important term of this methodology is the equilibrium point, which describes the steady state of the estimated parameters. For a better understanding equation (7) is considered. Here, the rest position is reached, when $i_{exc} = \hat{i}_{exc}$. In this case $R_{exc} = \hat{R}_{exc}$ under ideal conditions. From this view it follows

$$e_i=i_{exc}-\hat{i}_{exc} \tag{8}$$

and

$$e_R=R_{exc}-\hat{R}_{exc}. \tag{9}$$

The differentiation of equation (8) and (9) and the following insertion of equation (4) and (5) respectively equation (6) and (7) leads to

$$\frac{de_i}{dt}=-\frac{R_{exc}}{f_L}\cdot i_{exc}+\frac{\hat{R}_{exc}}{f_L}\cdot\hat{i}_{exc} \tag{10}$$

and

$$\frac{de_R}{dt}=-h_R\cdot e_i. \tag{11}$$

For the equations (8), (9), (10) and (11) a function $V(e_i,e_R)$ has to be found, which comply with the stability conditions of Lyapunov. According to [5] it is valid:

1. $V(e_i,e_R) > 0$ for $(e_i,e_R) \neq (0,0) \rightarrow$ positive definite
2. $V(0,0) = 0 \rightarrow$ positive definite
3. $\dot{V}(e_i,e_R) < 0 \rightarrow$ negative definite

The investigated function is

$$V(e_i,e_R)=\frac{1}{2}\cdot a\cdot e_i^2+\frac{1}{2}\cdot b\cdot e_R^2, \tag{12}$$

which is a circle for a = b and an ellipse for $a \neq b$. These two factors are freely selectable and serve for the adjustment of the dynamic of the nonlinear observer. It can be seen, that the stability conditions 1. and 2. are applicable for $a > 0$ and $b > 0$. The next step is the observation of $\dot{V}(e_i,e_R)$. It follows

$$\dot{V}(e_i,e_R)=a\cdot e_i\cdot\dot{e}_i+b\cdot e_R\cdot\dot{e}_R. \tag{13}$$

The insertion of equation (10) and (11) results in

$$\dot{V}(e_i,e_R)=-\left(a\cdot\frac{i_{exc}}{f_L}+b\cdot h_R\right)e_i\cdot e_R-a\cdot e_i^2\cdot\frac{\hat{R}_{exc}}{f_L}. \quad (14)$$

With the correct choice of h_R equation (14) can be simplified to one term. Therefore, the first term of equation (14) is set to 0 and gets converted to h_R, which leads to

$$h_R=-\frac{a}{b}\cdot\frac{i_{exc}}{f_L}. \quad (15)$$

The insertion of equation (15) in equation (14) results in

$$\dot{V}(e_i,e_R)=-a\cdot e_i^2\cdot\frac{\hat{R}_{exc}}{f_L}. \quad (16)$$

Stability condition 3. is fulfilled for $\hat{R}_{exc} > 0$ and $a > 0$. But it can be seen, that $\dot{V}(0)=0$. Therefore, $\dot{V}$ is only negative semi-idefinite. This means, that the equilibrium point is stable, but not asymptotically stable according to Lyapunov. With the aid of LaSalle's invariance principle [8] the asymptotic stability of the equilibrium point is proved. This principle will not be discussed in detail here.

IV. Simulation

In theory, the stability conditions of Lyapunov for equation (11) and (15) are fulfilled for the defined boundary conditions. However, an uncertainty exists, because of the equated denominators of equation (3) and (4). Hence, the simulation shall give information about the performance of the designed nonlinear observer in conjunction with the calculated correction factor h_R.

A. Simulink Model

Figure 10 shows the Simulink model of the nonlinear observer consisting of the parallel model of the excitation coil, the rotor resistance estimation and the calculation of the calculated excitation current $i_{exc,x}$ (green marked area), which is not used in the simulation.

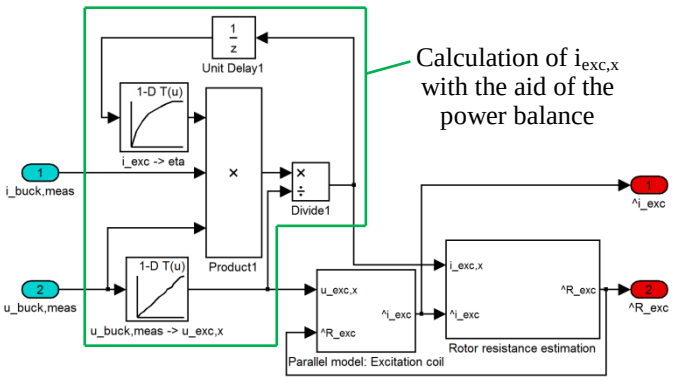

Figure 10: Simulink model of the Lyapunov-based nonlinear observer

The calculated excitation current is determined by the power balance of the CLL RW with the measured output voltage $u_{buck,meas}$ and the output current $i_{buck,meas}$ of the BC, the efficiency η_{CLL} of the CLL RW and the calculated excitation voltage $u_{exc,x}$. Thus, it follows

$$i_{exc,x}=\frac{u_{buck,meas}}{u_{exc,x}}\cdot i_{buck,meas}\cdot\eta_{CLL}. \quad (17)$$

Figure 11 presents the Simulink model of the parallel model of the excitation coil with the nonlinearity due to the excitation current dependent rotor inductance (blue marked area), which is described by the denominator of equation (3) respectively equation (4).

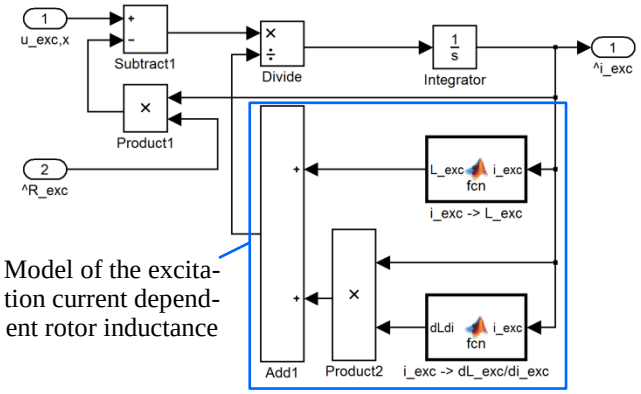

Figure 11: Simulink model of the parallel model of the excitation coil

The nonlinearity comprised the function of the absolute rotor inductance $L_{exc}(\hat{i}_{exc})$ and the function for the differential rotor inductance $dL_{exc}(\hat{i}_{exc})/d\hat{i}_{exc}$, which are determined by the polynomial interpolation according to Newton.

In Figure 12 the Simulink model of the rotor resistance estimation is shown. The calculated correction factor h_R (equation 15) is a part of this model (orange marked area).

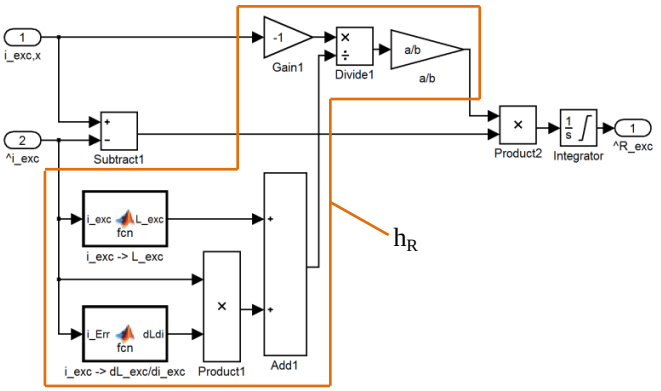

Figure 12: Simulink model of rotor resistance estimation

B. Simulation Results

In Figure 13 a simulation result of the calculated nonlinear observer for various initial values $\hat{i}_{exc}(0)$ and $\hat{R}_{exc}(0)$ is shown. It can be seen, that the progression of the estimated parameters (orange) converges to the true values (green) with Lyapunov stability.

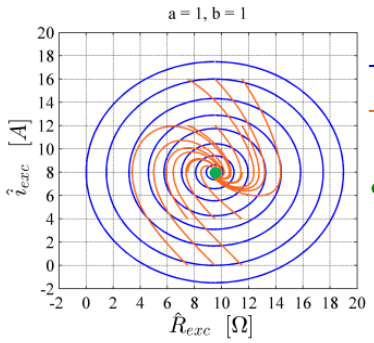

Figure 13: Simulation result of the Lyapunov-based nonlinear observer for different initial conditions

Figure 14 shows the simulation result of the exact linearization and the trajectory planning for a reference step of the excitation current from 3 A to13 A for the maximum excitation power $P_{exc,max}$ = 2 kW and a rotor resistance R_{exc} = 11,5 Ω.

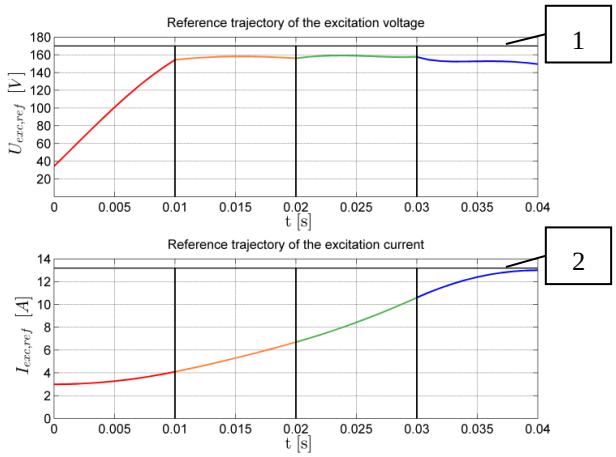

Figure 14: Simulation result of the exact linearization and the trajectory planning (1 – Defined excitation voltage boundary of 170 V, 2 – Max. reachable excitation current for $P_{exc,max}$ = 2 kW and R_{exc} = 11,5 Ω)

V. Hardware Components of the Inductive Energy Transfer System and Power Electronics

Figure 15 shows an exploded drawing and the hardware components of the IETS with the components for the integration in the EESM:

1 Heat sink with back mounted full bridge rectifier and smoothing capacitor
2 Housing for the protection of the rotating electronics
3 Adapter sleeve
4 Secondary ferrite core (rotating part of the transformer)
5 Clamping ring for the primary ferrite core
6 Primary ferrite core (fixed part of the transformer)
7 Rotor shaft with DC connection of the excitation coil (on the photo the rotor is extended → the line shows the place where the rotor normally stuck out)
8 End shield of the EESM.

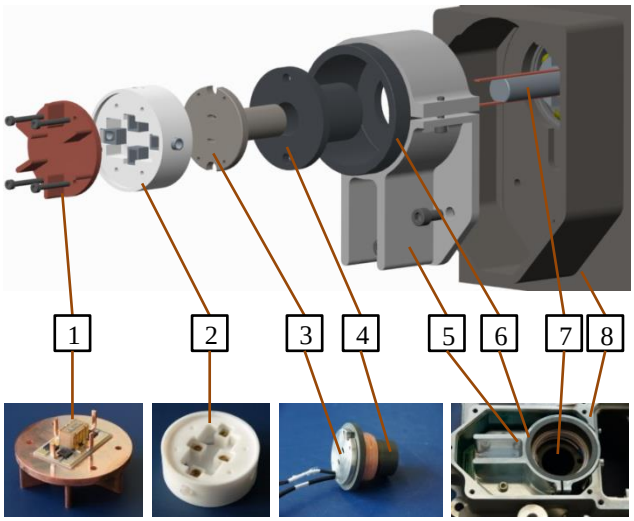

Figure 15: Exploded drawing of the IETS with the components for the integration in the EESM

Figure 16 shows the power electronics hardware of the IETS. It is connected to a dSpace realtime control system with the implemented Simulink model (controller, nonlinear observer etc.) by CAN bus to send and receive signals, for example the estimated excitation current (send) and the nominal value of the excitation current (receive).

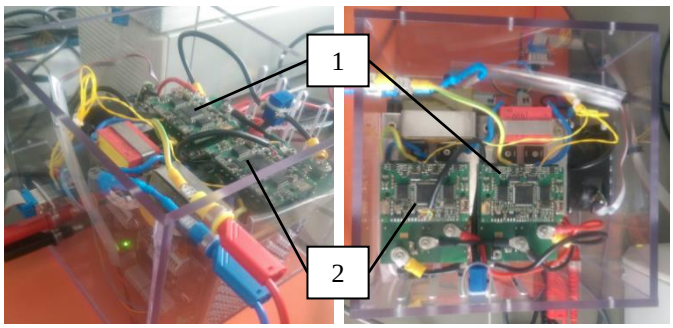

Figure 16: Power electronics of the inductive energy transfer system (1 – CLL RC, 2 – BC)

VI. Measurement Results

The measurement results are divided in the sections *Measurements in the Laboratory* and *Measurements on the Engine Test Bench*. In the laboratory it is possible to measure the excitation current and the rotor resistance for a comparison between the real and the estimated values. Thus, the control method can also be tested (trajectory generator, exact linearization, current controller for the excitation current, voltage controller for the output voltage of the BC). On the engine test bench the EESM can operate with a rotating rotor. Therefore, no load characteristics and torque measurements for different values of the excitation current can be made to make a comparison between the conventional EESM and the EESM with an IETS and a nonlinear observer. Thereby, it is possible to give a statement regarding to the accuracy of the excitation current and the generated torque.

A. *Measurements in the Laboratory*

Figure 17 and Figure 18 present the comparison of the real and the estimated excitation current as well as the comparison of the real and the estimated rotor resistance. The relative deviations for $\hat{\imath}_{exc}$ and $\hat{R}_{exc}$ regarding the maximum excitation current of 16 A are 2,96 % and -3,75 %. Hence, the nonlinear observer operates with a sufficient accuracy.

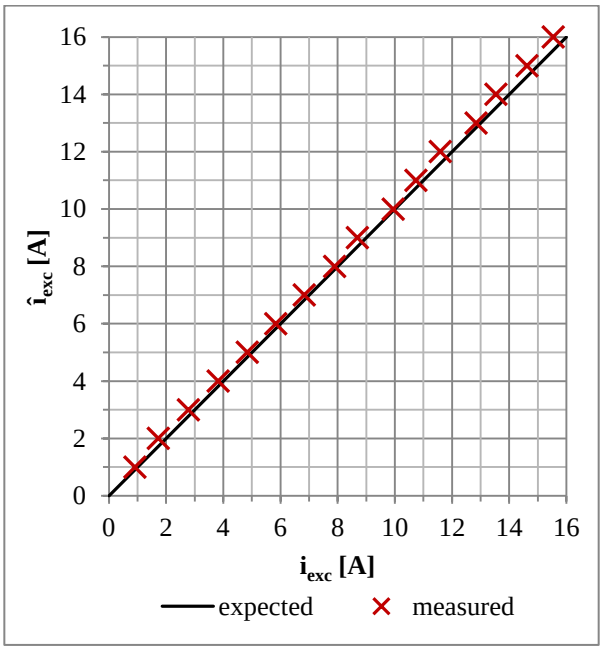

Figure 17: Estimation of the excitation current

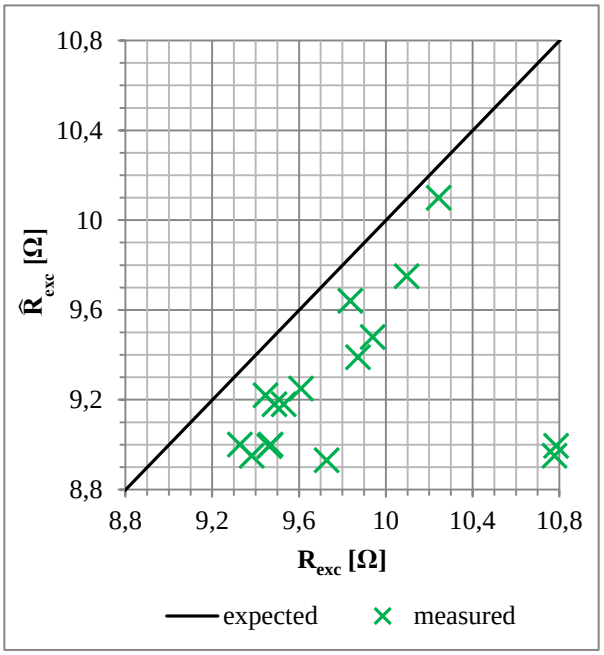

Figure 18: Estimation of the rotor resistance

In Figure 19 the increase of the estimated rotor resistance within 300 s due to a constant excitation current of 8 A is shown. The increase of the temperature leads to an increase of the real respectively the estimated rotor resistance, which causes a higher excitation voltage to retain the desired excitation current.

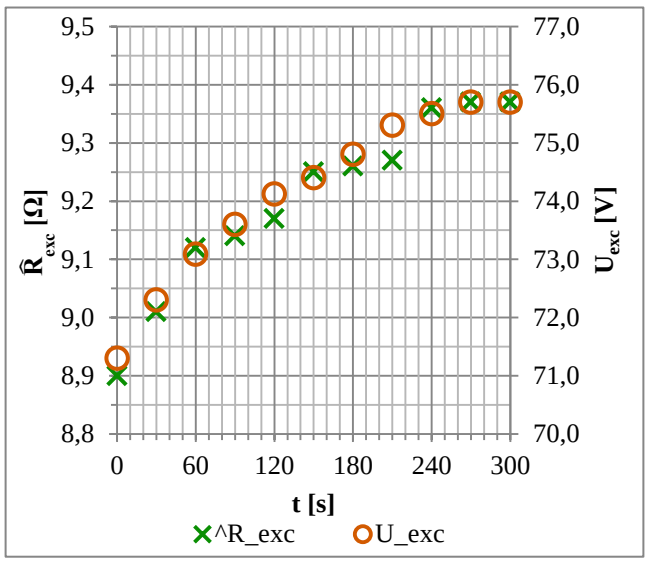

Figure 19: Increase of the estimated rotor resistance due to a constant excitation current of 8 A

Figure 20 shows a simulation result for the designed control method for a reference step of the excitation current from 3 A to16 A for a rotor resistance R_{exc} = 8 Ω.

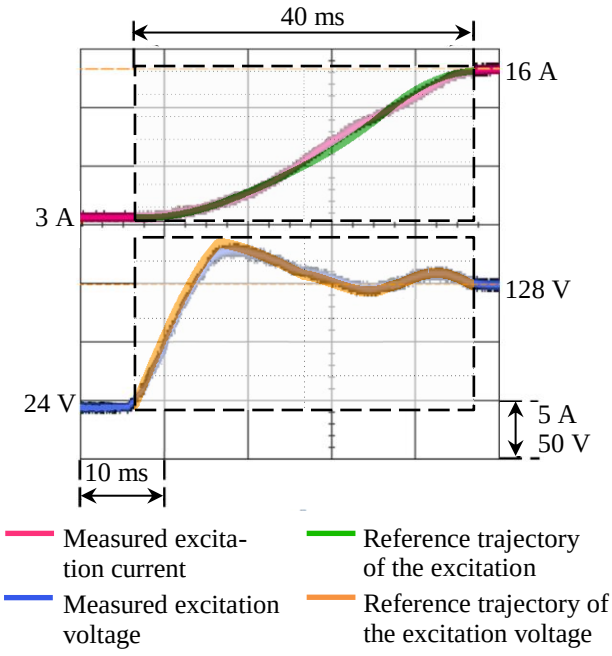

Figure 20: Comparison of the measured excitation current and the measured excitation voltage with their reference trajectories from the trajectory generator

With the aid of the developed trajectory generator and the exact linearization a good accordance between the measured signals and the reference trajectories is achieved.

B. Measurements on the Engine Test Bench

Figure 21 shows the comparison of the no load characteristics of the conventional EESM (o) and the EESM with an IETS and a nonlinear observer (x) to test the estimation current excitation. The parameter n_{TB} is the rotational speed at the driven end. Between the drive machine and the driven machine there is a gear ratio of 9,4, which has to be multiplied with n_{TB} to get the rotational speed of the rotor. This comparison shows, that there is a good accordance of the measured no load characteristics. However, the accuracy of the estimation current slightly decreases for higher rotational speeds, because the designed nonlinear observer does not consider n_{TB} respectively n_{rotor}.

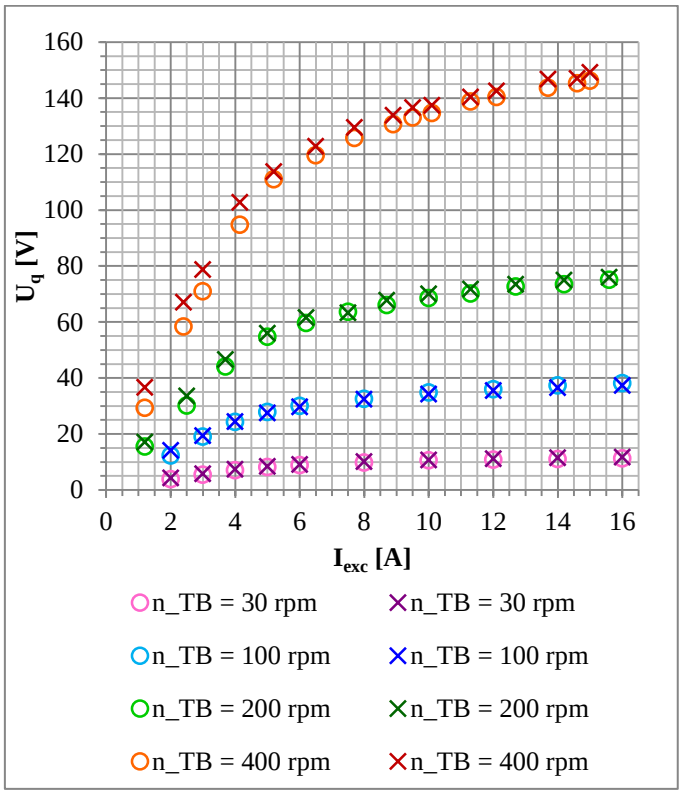

Figure 21: Comparison of the no load characteristics for different rotational speeds of the engine test bench to test the estimation of the excitation current – Conventional EESM (o), EESM with an IETS and a nonlinear observer (x)

In Figure 22 the comparison of the measured torque of the conventional EESM (o) and the EESM with an IETS and a nonlinear observer (x) for a rotational speed n_{TB} = 250 rpm and different values of I_q is shown (I_d = 0 A for all measured operating points). It can be seen, that there is a high accuracy achieved. The maximum deviation amounts -0,62 % for I_q = 133 A and -1,54 % for I_q = 266 A.

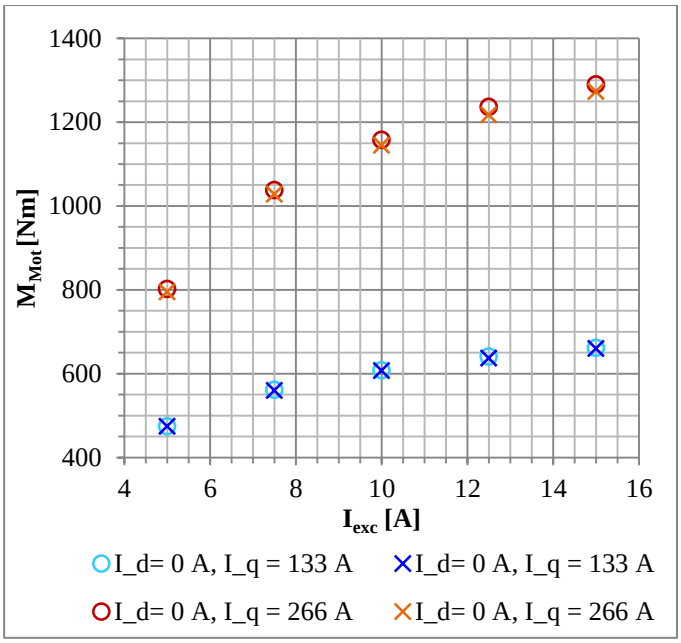

Figure 22: Comparison of the measured torque for a rotational speed n_{TB} = 250 rpm and different values of I_d - Conventional EESM (o), EESM with an IETS and a nonlinear observer (x)

VII. CONCLUSION

A Lyapunov-based nonlinear observer for the estimation of the excitation current and the rotor resistance of an EESM with an IETS has been designed. Regarding the maximum excitation current of 16 A, the designed estimation algorithm achieves an accuracy of more than 96 %. Therefore, this is a satisfactory result. With the development of the described IETS the slip rings of the EESM can be removed. There is no mechanical wear respectively abrasion in the air gap and consequently, there are no high voltage insulation problems by using this contactless method.

REFERENCES

[1] W. Hackmann, B. Wagner, R. Zwingel, I. Dziedzek, K. Welke, „Fremderregte Synchronmaschinen im Einsatz als Achshybridantriebe“, International ETG Congress, Karlsruhe, Germany, pp. 55-64, Oct. 2007

[2] S. Köhler, „Erregerstrom- und Rotortemperaturschätzung einer durch einen DC-DC-Wandler gespeisten fremderregten Synchronmaschine“, Master Thesis, TH Nürnberg GSO: Nuremberg, Nov. 2014

[3] A. Littau, B. Wagner, S. Köhler, A. Dietz, S. Weber, „Design of Inductive Power Transmission into the Rotor of an Externally Excited Synchronous Machine“, CoFat, Munich, March 2014

[4] M.-K. Kazimierczuk, D. Czarkowski, „Resonant Power Converters”, Hoboken: Wiley, pp. 448-457, 2011

[5] R. Beiranvand, M. R. Zolghadri, S. M. H. Alavi, „Using LLC Resonant Converter for Designing Wide-Range Voltage Source“, IEEE Transactions on Industrial Electronics, Vol. 58, No. 5, pp. 1746-1756, May 2011

[6] A. Isidori, „Nonlinear Control Systems: An Introduction“, Heidelberg: Springer-Verlag, pp. 178-253, 1985

[7] A. N. Michel, L. Hou, D. Liu, „Stability of Dynamical Systems – Continuous, Discontinuous and Discrete Systems“, Boston: Birkhäuser Boston, pp. 199-211, 2008

[8] J. Adamy, “Nichtlineare Systeme und Regelungen”, Heidelberg: Springer Vieweg, 2. Edition, pp. 101-104, 2014